Journal of the Mechanics and Physics of Solids 143 (2020) 103988

Contents lists available at ScienceDirect

Journal of the Mechanics and Physics of Solids

journal homepage: www.elsevier.com/locate/jmps

Strength and toughness of adhesion of soft materials measured in lap shear

Yecheng Wang[a], Xuxu Yang[a,b], Guodong Nian[a], Zhigang Suo[a,*]

[a] John A. Paulson School of Engineering and Applied Sciences, Kavli Institute for Bionano Science and Technology, Harvard University, MA 02138, United States

[b] Department of Engineering Mechanics, Zhejiang University, Hangzhou 310027, China

ARTICLE INFO

Article history:
Received 16 February 2020
Revised 18 April 2020
Accepted 19 April 2020
Available online 9 June 2020

Keywords:
Adhesion
Lap shear
Strength
Toughness
Hydrogel

ABSTRACT

Adhesion of soft materials is commonly characterized by strength and toughness. Their applicability, however, is often questionable even for widely used test methods. Here we study lap shear using a combination of experiment, theory, and computation. Lap shear has long been used to measure adhesion strength of soft materials, but our experiments show that the measured adhesion strength is constant only when the sample is thin and short enough. When the sample thickness exceeds the fractoadhesive length, the corner of the sample concentrates stress, and the adhesion strength decreases as the sample thickness increases. When the sample length exceeds the shear lag length, the backing layer deforms appreciably, much of the sample does not carry shear stress, and the adhesion strength decreases as the sample length increases. Furthermore, we derive an analytical expression for energy release rate for a crack long compared to the sample thickness. For samples thicker than the fractoadhesive length, we show that the adhesion toughness is constant, independent of the sample length. These findings will guide the development of the methods to characterize strength and toughness of adhesion.

1. Introduction

The art of adhesion dates back to antiquity, and has long been developed for hard and dry materials, such as wood, metals, and ceramics (Ebnesajjad and Landrock, 2014; Skeist, 1990). In recent years, much attention has been devoted to the development of methods of adhesion for soft and wet materials, such as living tissues and hydrogels (Mehdizadeh and Yang, 2013; Yang et al., 2019c). Adhesion of soft and wet materials—either among themselves or to hard and dry materials—has been achieved through covalent interlinks (Li et al., 2017, 2019; Liu et al., 2018; Yuk et al., 2015, 2016), noncovalent (supramolecular) interlinks (Rose et al., 2014; Roy et al., 2015; Wang et al., 2019a), and topological entanglement (Gao et al., 2018; Steck et al., 2019; Yang et al., 2018).

The rapid advances of adhesion of soft and wet materials have promising applications in engineering and medicine. Examples include wound closure (Blacklow et al., 2019; Hong et al., 2019; Li et al., 2017; Yuk et al., 2019), hydrogel paint (Yao et al., 2019), hydrogel skin (Yu et al., 2019), hydrogel robot (Yuk et al., 2017), high-toughness, low-hysteresis elastomers (Wang et al., 2019b), fatigue-resistant stretchable materials (Li et al., 2020; Xiang et al., 2019), strong and tough soft composite (Huang et al., 2017), photodetachable adhesion (Gao et al., 2018), molecular staple (Chen et al., 2019; Wirthl et al.,

* Corresponding author.
E-mail address: suo@seas.harvard.edu (Z. Suo).

https://doi.org/10.1016/j.jmps.2020.103988
0022-5096/

2017), strong and degradable adhesion (Yang et al., 2019b), stick-on large-strain sensors (Cheng et al., 2019), and topological prime and topological lithography (Yang et al., 2020).

Materials adhere and detach through complex molecular processes. The quality of adhesion is assessed not by first-principles computations, but by mechanical tests. Typical tests include probe pull, lap shear, and peel. Probe pull and lap shear are commonly used to measure adhesion strength, whereas peel is commonly used to measure adhesion toughness. In particular, lap shear has been widely used to characterize structural adhesives (Jeevi et al., 2019) and tissue adhesives (Ni et al., 2019; Roy et al., 2015; Vakalopoulos et al., 2015; Yuk et al., 2019). Adhesion strength and adhesion toughness are used to rank adhesion of various chemistries (Bhagat and Becker, 2017; Hofman et al., 2018; Zhu et al., 2018), as well as various microstructures (Ghareeb and Elbanna, 2019; Xia et al., 2012).

The applicability of strength and toughness is inadequately appreciated. To illustrate concerns and resolutions, this paper reports several findings of lap shear of hydrogels. We use the adhesion between polyacrylic acid hydrogel and polyacrylamide hydrogel as a model system. Our experiment shows that the adhesion strength changes with the sample thickness when the sample thickness is large compared to the fractocohesive length, and changes with the sample length when the sample length is large compared to the shear lag length (Section 2). For thick samples, a combination of theory, computation, and experiment shows that lap shear gives geometry-independent adhesion toughness (Section 3 and Section 4). We also compare the lap shear using flexible backing layers and that using rigid substrates (Section 5). We describe the experimental approaches and show the force-displacement curves of various thicknesses and lengths (Section 6). These findings will guide the characterization of strength and toughness in developing and applying methods of adhesion in engineering and medicine, as well as contribute to the fundamental mechanics of adhesion.

2. Adhesion strength

2.1. Lap shear

Lap shear is commonly used to measure adhesion strength (da Silva et al., 2006; Hui et al., 2018; Kafkalidis and Thouless, 2002; Kendall, 1975; Liu et al., 2019b). As a typical example, structural adhesive has been extensively studied by lap shear and the effects of overlap length, bond line thickness, and other parameters on joint strength have been reported (da Silva et al., 2006; Grant et al., 2009; Kendall, 1975; Taib et al., 2006). For structural adhesives, both adherends and adhesives are stiff and the deformation is small. By contrast, for soft adhesive joints, the modulus between the soft layer and the stiff backing layer differs by orders of magnitude and the deformation in the soft layer is finite. As we will see later, the enormous modulus contrast leads to a very long shear lag length.

Here, we lap-shear an adhesive joint made of polyacrylic acid (PAA) hydrogel and polyacrylamide (PAAm) hydrogel (Fig. 1a). Values of thickness of each hydrogel are identical, $h/3$. Following an existing practice, define the adhesion strength by

$$\tau_s = \frac{F_{max}}{wL}, \tag{1}$$

where F_{max} is the maximum force in the force-displacement curve (Fig. 1b), and w and L are the width and length of the area of adhesion, respectively. When a loading machine pulls the two backing layers, the sample rotates somewhat, deforms greatly, and then ruptures (Fig. 1c, Video 1).

Definition (1) makes sense only when the stress in the adhesive joint is uniform. This assumption is unrealistic in practice, where the corner of the adhesive joint may concentrate stress (Fig. 1c). Nonuniform stress in lap shear has been studied (da Silva et al., 2009a, 2009b; Kafkalidis and Thouless, 2002). However, most existing models have no analytical solutions and are rarely used in practice. By contrast, the simple but "unrealistic" definition (1) has been widely adopted, following the ASTM D1002-10 (metals), ASTM D3163-01 (plastics), and ASTM F2255-05 (tissue adhesives). In this paper, we will adopt the simple definition to report adhesion strength.

We measure adhesion strength for samples of various values of thickness h (Fig. 1d), while fixing the length $L = 5$ cm and the width $w = 2$ cm. We find that the adhesion strength is constant when the sample thickness is below a certain thickness, but decreases when the sample is thick.

We also measure adhesion strength for samples of various values of length L (Fig. 1e), while fixing the thickness $h =$ 9 mm and the width $w = 2$ cm. We find the adhesion strength is constant when the sample length is below a critical length, but decreases when the sample is long.

2.2. Fractoadhesive length

To study the thickness dependence of the adhesion strength, we invoke the fractocohesive length defined as (Chen et al., 2017)

$$R_f = \frac{\Gamma}{W_f}. \tag{2}$$

The fractocohesive length is characteristic of a homogeneous material, where Γ is the toughness of the material measured using a sample containing a pre-cut crack, and W_f is the work of fracture of the material measured using a sample without

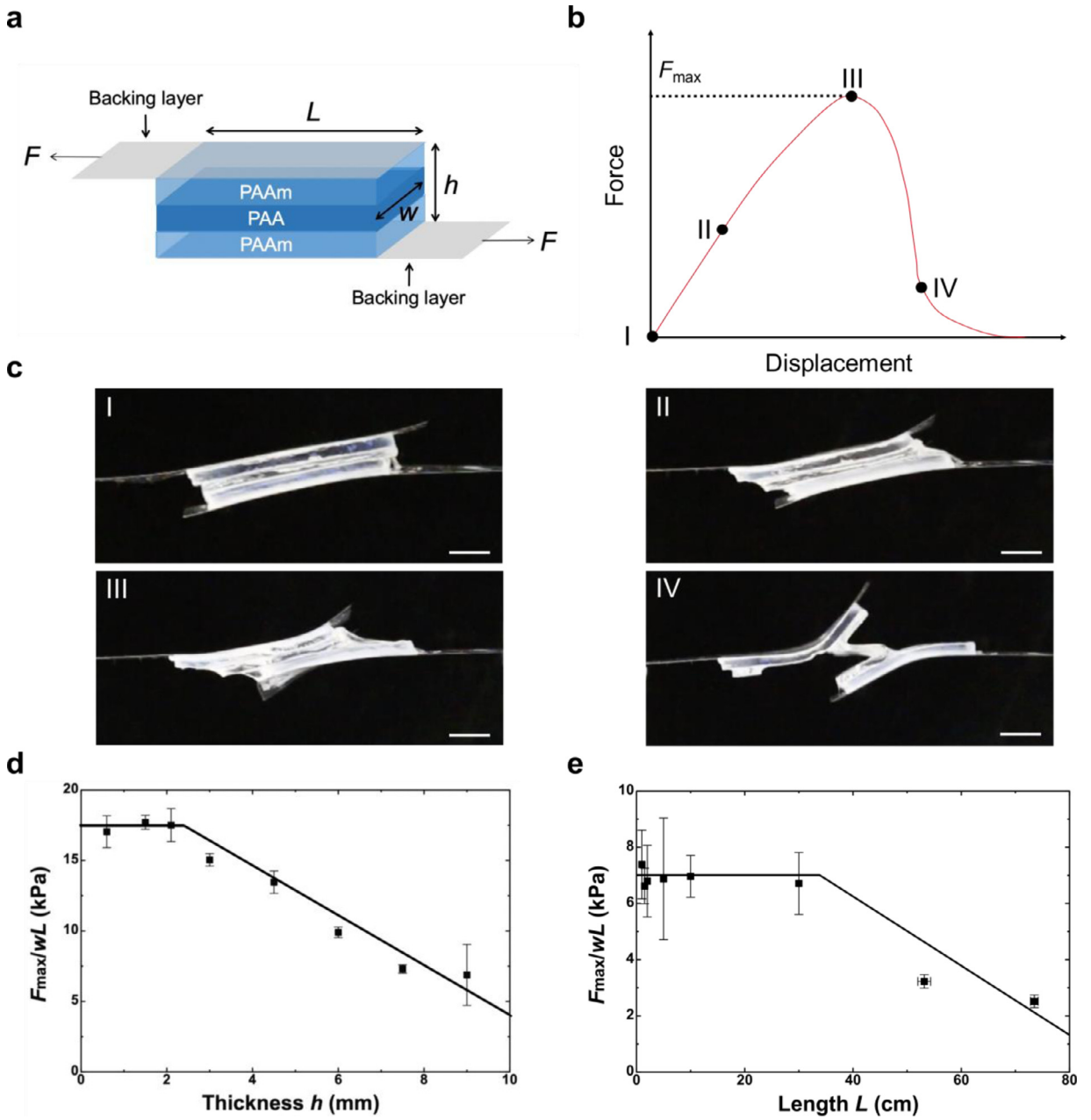

Fig. 1. Use lap shear to measure adhesion strength. (a) Experimental setup. Two polyacrylamide hydrogels (pH = 3.5) sandwich a polyacrylic acid hydrogel (pH = 1.5), and form an adhesive joint, of length L, width w, and thickness h. Unless otherwise specified, the width w is fixed as 2 cm. The adhesive joint is pulled using two plastic backing layers, which are glued to the polyacrylamide hydrogels. (b) Force-displacement curve. Shear strength is defined as the maximum force divided by the initial area of the adhesive joint. (c) Images of a sample at various positions in the force-displacement curve. Scale bar is 1 cm. (d) The measured adhesion strength depends on the sample thickness. The length $L = 5$ cm. (e) The measured adhesion strength depends on the sample length. The thickness $h = 9$ mm. In (d) and (e), solid lines are drawn to guide the eye.

pre-cut crack. In an experiment with a large sample and a long pre-cut crack, a fracture process zone exists around the crack tip. The sample is elastic outside the fracture process zone. The fractocohesive length scales the fracture process zone. The fractocohesive length is ~ 1 mm for PAA and PAAm hydrogels (Liu et al., 2019a; Yang et al., 2019a).

Here we define a similar length to characterize adhesion, which may be called the fractoadhesive length. The two hydrogels used in our experiments adhere well, and the adhesive fracture between the two hydrogels is comparable to the cohesive fracture of the two hydrogels (Wang et al., 2019a). Consequently, here we will simply adopt the fractoadhesive length of ~ 1 mm to evaluate PAA-PAAm adhesion.

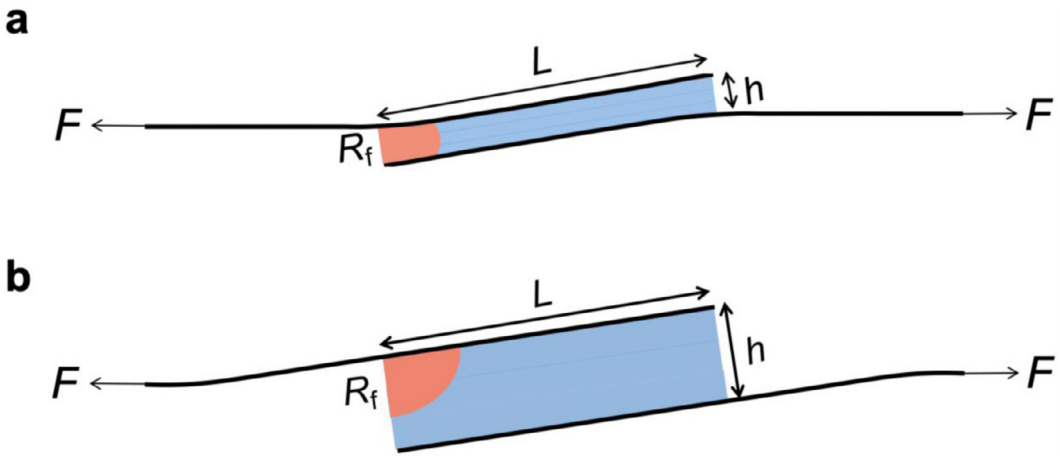

Fig. 2. Scale of inelasticity. (a) When $h < R_f$, the effect of stress concentration is negligible. (b) When $h > R_f$, the effect of stress concentration is significant.

2.3. Adhesion strength changes with the sample thickness

When no intentional pre-cut crack is made, unintentional crack-like flaws introduced during material synthesis are likely to be smaller than the fractocohesive length of ~ 1 mm. In lap shear, we compare the fractocohesive length R_f with the thickness h of the sample. When $h < R_f$, the fracture process zone expands across the thickness of the sample, so that the effect of stress concentration is negligible (Fig. 2a). By contrast, when $h > R_f$, the fracture process zone is small compared to the sample thickness, so that the effect of stress concentration becomes pronounced (Fig. 2b).

The experimental results are consistent with the scale of inelasticity (Fig. 1d). When $h < R_f$, the effect of stress concentration is negligible, and the shear strength is independent of the sample thickness. When $h > R_f$, the effect of stress concentration is pronounced, and the shear strength decreases as the sample thickness increases.

2.4. Shear lag length

To study the length dependence of the adhesion strength, we employ the shear lag model (Cox, 1952; Hui et al., 2018; Mojdehi et al., 2017). Here we only need to find the length scale over which the shear stress in the soft material vanishes. To estimate this shear lag length, consider a soft layer sandwiched between an elastic backing layer and a rigid foundation. Let E and H be the Young's modulus and thickness of the backing layer, and μ and h be the shear modulus and thickness of the soft layer. Let x be the coordinate along the length of the sample, $\sigma(x)$ be the tensile stress in the backing layer, $u(x)$ be the shear displacement of the backing layer relative to the foundation, and $\tau(x)$ be the shear stress in the soft material. The balance of forces requires that $H\mathrm{d}\sigma(x)/\mathrm{d}x = \tau(x)$. The elasticity requires that $\mathrm{d}\sigma(x) = E\mathrm{d}u(x)/\mathrm{d}x$ and $\tau(x) = \mu u(x)/h$. A combination of the three equations gives that $\mathrm{d}^2u(x)/\mathrm{d}x^2 = [\mu/(EHh)]u(x)$. This second-order ordinary equation defines a length scale (i.e., the shear lag length):

$$L_s = \sqrt{\frac{EHh}{\mu}}. \tag{3}$$

Taking H ~ 100 μm, E ~ 1 GPa, h ~ 1 mm, and μ ~ 1 kPa, we can estimate the shear lag length $L_s \approx 31.6$ cm.

2.5. Adhesion strength changes with the sample length

We compare the shear lag length L_s with the length L of the sample. When $L \ll L_s$, the soft layer carries stress and undergoes a homogeneous deformation, so that the effect of the backing layer elasticity is negligible (Fig. 3a). By contrast, when $L \gg L_s$, much of the soft layer carries negligible stress but the backing layer carries stress, so that the elasticity of the backing layer becomes pronounced (Fig. 3b).

The experimental results are consistent with the load transfer (Fig. 1e). When $L \ll L_s$, the effect of the backing layer elasticity is negligible, and the adhesion strength is independent of the sample length. When $L \gg L_s$, the backing layer deforms appreciably, and the adhesion strength decreases as the sample length increases.

To further confirm the significance of the shear lag length, we calculate the shear stress of the top layer of the soft layer, τ, normalized by the average shear stress, F/wL, along the length direction x of various normalized sample lengths, L/L_s, using the finite element software ABAQUS (Fig. 4).

A prescribed displacement is applied to the left end of the upper backing layer and the right end of the other backing layer is fixed during tension. 4-node bilinear plane strain quadrilateral elements (CPE4R) are adopted for both the backing

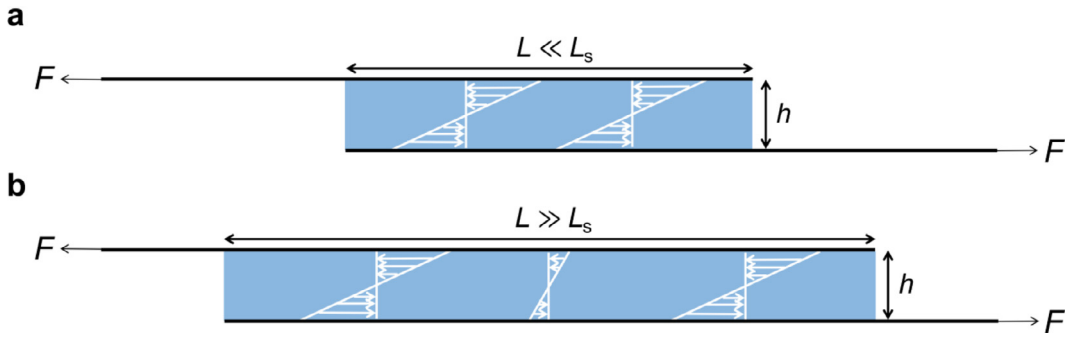

Fig. 3. (a) When $L \ll L_s$, the effect of backing layer elasticity is negligible. (b) When $L \gg L_s$, the effect of backing layer elasticity is significant.

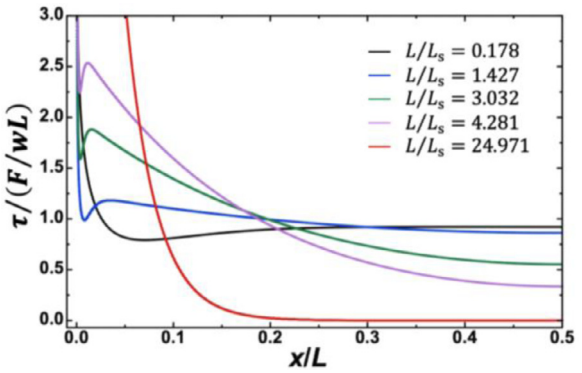

Fig. 4. Normalized shear stress $\tau/(F/wL)$ distribution of the top layer of the soft layer along the direction of length x of various normalized sample lengths L/L_s.

layers and the hydrogel. The backing layer is assumed to be linear elastic, and the hydrogel is neo-Hookean. This elastic model cannot correctly represent the stress concentration at the corner of the sample, so we will ignore the prediction of the high stress near the corner. The elastic model, however, should adequately model the stress in the soft layer at some distance away from the corner. When $L < L_s$, the shear stress is nearly uniformly distributed along the direction of length and is well approximated by $\tau = F/wL$. When $L > L_s$, the shear stress decreases as the length L increases, so that $\tau \ll F/wL$.

3. Adhesion toughness for short samples

Strength and toughness are independent properties (Ritchie, 2011). Strength is the maximum stress a material can sustain, describing the ability of a material without cracks to resist fracture. By contrast, toughness is the amount of energy needed for a crack to propagate per unit area, reflecting the ability of a material with cracks to resist crack growth. Similar comments apply to the strength and toughness of the adhesion between two materials. As shown in the previous section, the measured adhesion strength is thickness-dependent in the range of $h > R_f$ (Fig. 1d). To resolve this issue, we use thick samples to measure adhesion toughness. In this section, we study adhesion toughness for short samples, $L \ll L_s$, when the backing layer can be assumed to be rigid.

3.1. Steady-state energy release rate

To measure adhesion toughness, one introduces a pre-cut crack into the sample, and relates the energy release rate of the crack to the applied load and sample geometry. We use the theory of nonlinear elasticity to calculate a steady-state energy release rate for a soft elastic layer undergoing finite deformation (Fig. 5). A soft elastic layer, thickness h, is sandwiched between two rigid substrates. Assume that the elastic layer is made of a homogeneous material. Part of the elastic layer, length l_1, detaches from a substrate, and the other part of the elastic layer, length l_2, adheres to both substrates. The boundary between the detached and adhered parts is taken to be the crack front. The thickness of the elastic layer, h, is taken to be small compared to both l_1 and l_2. When one rigid substrate slides relative to the other, the adhered part of the elastic layer undergoes a homogeneous deformation of a shear strain γ, the detached region does not deform, and only a small region around the front of the crack undergoes inhomogeneous deformation. Consequently, the crack is in steady state. By definition, the energy release rate G is the reduction of the elastic energy associated with the crack advancing per

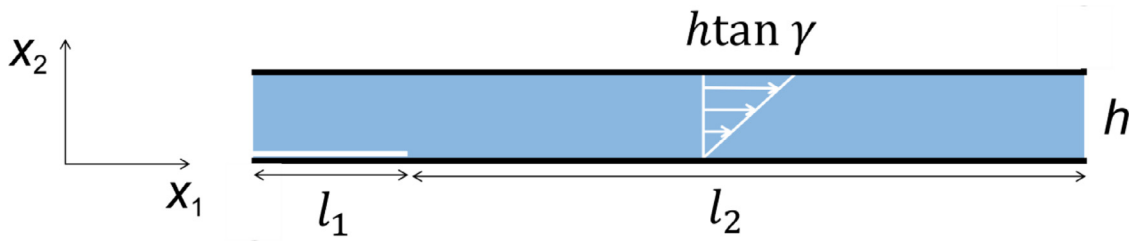

Fig. 5. An idealized model for the derivation of the steady-state energy release rate.

unit area, so that

$$G = hW(\gamma), \tag{4}$$

where $W(\gamma)$ is the elastic energy of the deformed layer per unit volume. This result is independent of specific model of elasticity. The above expression is expected to be valid when both l_1 and l_2 are large compared to the thickness of the elastic layer, h. Under this condition, the energy release rate is independent of l_1 and l_2, and is said to reach a steady state.

We next focus on the homogeneous shear deformation in the part of the elastic layer adhered to both substrates. In the undeformed state, consider a vertical line of material particles. In the deformed state, the same line of material particles rotates by an angle of γ. In the undeformed state, label each material particle by its coordinates (X_1, X_2, X_3), where the axis X_1 coincides with the bottom of the elastic layer, X_2 is normal to the elastic layer, and X_3 coincides with the crack front. When the top substrate slides relative to the bottom substrate by a rigid-body translation of $h\tan\gamma$, the material particle of coordinates (X_1, X_2, X_3) in the undeformed state moves to a place of coordinates (x_1, x_2, x_3) in the deformed state, where $x_1 = X_1 + X_2\tan\gamma$, $x_2 = X_2$, and $x_3 = X_3$. Consequently, the deformation gradient, $F_{iK} = \partial x_i(X_1, X_2, X_3)/\partial X_K$, is

$$\mathbf{F} = \begin{bmatrix} 1 & \tan\gamma & 0 \\ 0 & 1 & 0 \\ 0 & 0 & 1 \end{bmatrix}. \tag{5}$$

The elastic layer is taken to obey the neo-Hookean model of the energy density $W(\mathbf{F}) = \frac{\mu}{2}(F_{iK}F_{iK} - 3)$, where μ is the shear modulus. When the material is deformed with a shear strain γ, the elastic energy density of the neo-Hookean material is $W = \mu(F_{12})^2 = \mu\tan^2\gamma/2$. Thus, for a neo-Hookean material, the energy release rate is $G = h\mu\tan^2\gamma/2$.

We next ascertain that a homogeneous shear deformation indeed satisfies the boundary conditions of lap shear. The elastic layer is further assumed to be incompressible, $\det\mathbf{F} = 1$. For an elastic, incompressible material, the true stress is expressed by the energy density as

$$\sigma_{ij} = \frac{\partial W(\mathbf{F})}{\partial F_{iK}}F_{jK} - \Pi\delta_{ij}, \tag{6}$$

where the Lagrange multiplier Π is introduced to enforce incompressibility. For the neo-Hookean material, the stress-strain relation reduces to $\sigma_{ij} = \mu F_{iK}F_{jK} - \Pi\delta_{ij}$. Under shear, the stress tensor is

$$\sigma_{12} = \mu\tan\gamma, \ \ \sigma_{23} = \sigma_{31} = 0, \ \ \sigma_{11} = \sigma_{22} = \sigma_{33} = \Pi. \tag{7}$$

The Lagrange multiplier Π gives a state of hydrostatic stress, which is set by the atmospheric pressure in our experiment. The hydrostatic stress does not affect the elastic energy for an incompressible material. At free edges of the sample, the shear stress is absent. This boundary condition violates the result $\sigma_{12} = \mu\tan\gamma$, but is assumed to affect only a small region near each edge.

When the two substrates slide under an applied force, assuming that the attached region undergoes a homogeneous deformation, the shear stress is given by $\sigma_{12} = \tau$, where the shear stress τ is the force applied on the substrate divided by the attached area. The steady-state energy release rate is $G = h\tau^2/2\mu$. This result is valid for lap shear with arbitrarily large deformation, so long as the elastic material is neo-Hookean, the crack length is large compared to the sample thickness, and the substrates are rigid. Furthermore, even if the forces applied to the rigid substrates have components normal to the elastic layer, the normal forces will contribute to the hydrostatic stress in the incompressible, thin, elastic layer, but will not cause any deformation, and will not affect energy release rate. When a force is applied normal to the thin soft layer, the applied tensile force will affect mode mix at the crack front, even though the energy release rate is unaffected. Thus, the validity of $G = h\tau^2/2\mu$ is remarkably general.

In our experiment, the elastic layer consists of a PAA hydrogel and two PAAm hydrogels. Both PAA and PAAm have the thickness of $h/3$. The shear stress τ is the same in all three layers, but the shear strains are different in PAA and PAAm, because the two materials have dissimilar shear moduli, μ_{PAAm} and μ_{PAA}. Hence, the steady-state energy release rate is

$$G = \left(\frac{h}{3\mu_{PAAm}} + \frac{h}{6\mu_{PAA}}\right)\tau^2. \tag{8}$$

Define an effective shear modulus $\bar{\mu}$ by $1/\bar{\mu} = 2/3\mu_{PAAm} + 1/3\mu_{PAA}$, and write the above equation as $G = h\tau^2/2\bar{\mu}$.

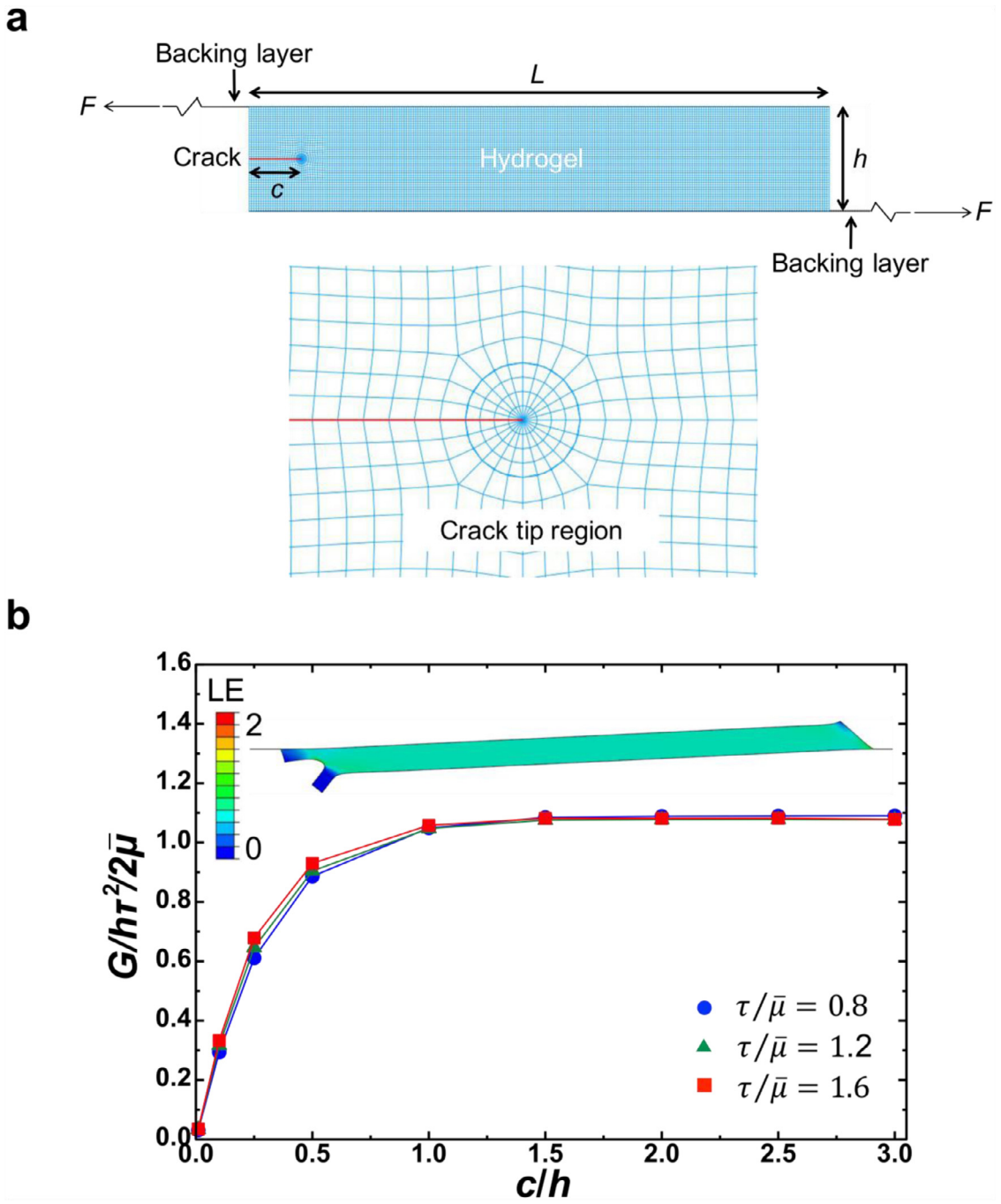

Fig. 6. Finite element analysis. (a) Finite element model for lap shear and the refined mesh near the crack tip. (b) Dimensionless analysis. Normalized energy release rate $G/h\tau^2/2\bar{\mu}$ is plotted as a function of normalized crack length c/h at various normalized shear stresses $\tau/\bar{\mu}$. Inset: maximum principal logarithmic strain (LE) fields when $c/h = 1$ and $\tau/\bar{\mu} = 1.2$.

3.2. Finite element analysis of the effect of the crack length

The above result applies to a steady-state crack, when the crack length is large compared to the sample thickness. Next, we calculate the energy release rate for a transient crack using the finite element software ABAQUS. Let c be the length of the crack, and the object here is to determine the length of the crack to approach the steady-state energy release rate. To simplify the calculation, we replace the three-layered composite by a homogeneous hydrogel. We use contour integrals to calculate the energy release rate. A two-dimensional finite element model is employed (Fig. 6a). A prescribed displacement

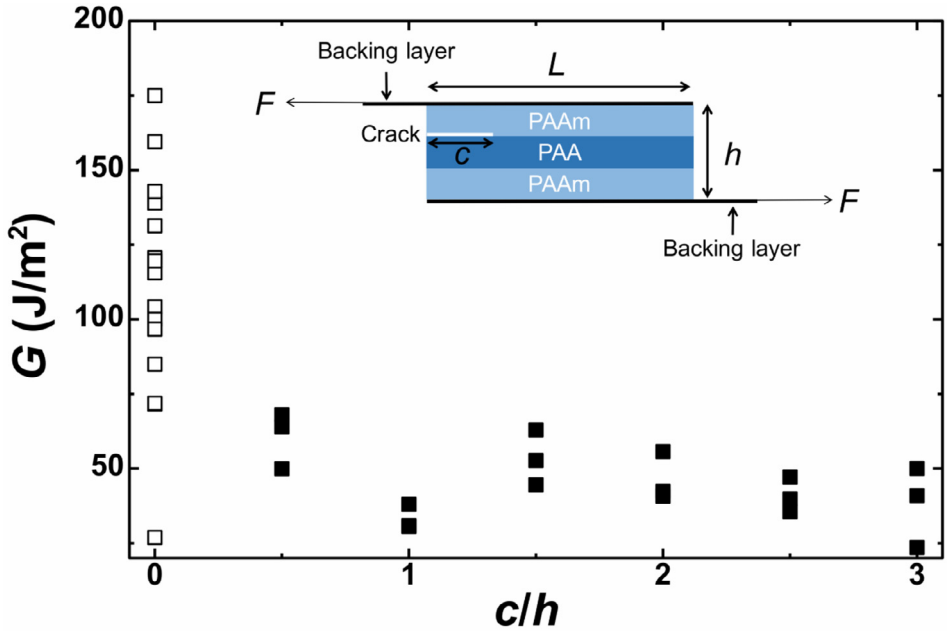

Fig. 7. Adhesion toughness measurement. An initial crack with various lengths is introduced to the PAA-PAAm interface, and the corresponding maximum forces are measured. Inextensible backing layers are glued to PAAm hydrogels to suppress their deformation far away from the crack. In this case, $h = 9$ mm $> R_f$, $L = 5$ cm, and $w = 2$ cm. Also included in the figure are data (the empty squares) measured using samples with no pre-cut crack.

is applied to the left end of the upper backing layer and the right end of the other backing layer is fixed during tension. 4-node bilinear plane strain quadrilateral elements (CPE4R) are adopted for both the backing layers and the hydrogel except for the crack tip region, where the crack-tip singularity is modeled with a ring of collapsed quadrilateral elements. To obtain the desired accuracy, the mesh close to the crack is refined. In the calculation, the backing layers are assumed to be linear elastic. The length and thickness of each backing layer are 75 cm and 50 μm, respectively. For the hydrogel, the neo-Hookean model is adopted, and its shear modulus is 2.634 kPa. In addition, the length L is kept to be 10 cm, and the thickness h is 4.5 mm, which is large compared to the fractocohesive length R_f.

The results show that when the crack length is comparable to the sample thickness, the energy release rate reaches a steady state (Fig. 6b). The finite element analysis also confirms that the strain is uniform in the main part of the sample. The calculated normalized energy release rate at steady state is slightly higher than the theoretical prediction $G = h\tau^2/2\tilde{\mu}$. This difference is caused by the finite elastic modulus of the backing layers assumed in the finite element analysis (Appendix A). The above results corroborate the validity of the use of the steady-state energy release rate $G = h\tau^2/2\tilde{\mu}$ when the crack length exceeds the sample thickness.

3.3. Experimental measurement of adhesion toughness

We experimentally measure the adhesion toughness by introducing a crack to the interface between PAA and PAAm with a crack length c (Fig. 7).

We fix the length $L = 5$ cm and the width $w = 2$ cm. To guarantee that fracture is limited by toughness, we make $h = 9$ mm, which is large compared to R_f. The results show that a steady state is reached and the energy release rate is independent of the crack length. According to the finite element analysis (Fig. 6b), a steady state is reached when $c/h \geq 1$. Thus, we can obtain the steady-state energy release rate when $c/h \geq 1$, using Eq. (8). For $c/h = 0.5$, the energy release rate is calculated using Eq. (8) with a coefficient of 0.9. The average energy release rate at steady state is 45 J/m^2. By uniaxial tension test, we can determine Young's modulus of PAAm and PAA. The materials are taken to be incompressible, so that Young's modulus divided by 3 gives the shear modulus, $\mu_{PAAm} = 4256 \pm 238$ Pa and $\mu_{PAA} = 1495 \pm 58$ Pa. Taking $h = 9$ mm and $\tau = 5$ kPa (Fig. 7), we can estimate the adhesion toughness $\Gamma \approx 43$ J/m^2, which is consistent with the experimental measurement.

To illustrate the importance of the pre-cut crack in the measurement of toughness, we calculate the energy release rate of the cases when $h > R_f$ in Fig. 1d using Eq. (8). The results (empty squares in Fig. 7) show large scatters. The scatters are due to the uncertainty of the crack length caused by the absence of pre-cut crack. Therefore, a pre-cut crack long compared to the thickness is necessary to measure adhesion toughness using the steady-state energy release rate.

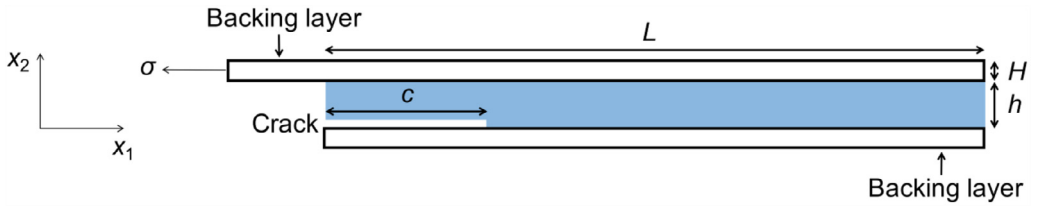

Fig. 8. Energy release rate for a crack in a long sample.

4. Adhesion toughness for long samples

As shown in the previous sections, the adhesion toughness for short samples is constant. In this section, we study the case of long samples and show adhesion toughness is constant and consistent with that of short samples. For a long sample, $L \gg L_s$, the elasticity of the backing layers strongly affects the energy release rate.

4.1. Steady-state energy release rate

We now calculate the energy release rate due to the elasticity of the backing layer (Fig. 8). A soft elastic layer, thickness h, is sandwiched between two stiff backing layers, thickness H. We assume that the soft elastic layer is made of a homogeneous material. The thickness of the soft elastic layer, h, is taken to be small compared to the length of the soft elastic layer, L. Let w be the width of the sample. A crack of a length c is introduced between the soft elastic layer and the stiff backing layer. The backing layers are pulled by the force F. In the detached part, far behind the crack front, only one backing layer carries stress, $\sigma = F/wH$, and the elastic energy per unit length of the backing layer is $H\sigma^2/2E$. In the adhered part, far ahead the crack front, both the backing layers carry stress, so that the stress in each backing layer is $\sigma/2$, and the elastic energy per unit length of the two backing layers is $H(\sigma/2)^2/E$. The difference in the elastic energy per unit length between the two parts gives the energy release rate:

$$G = \frac{H\sigma^2}{4E}. \tag{9}$$

We have obtained analytical expressions of energy release rate in two limits. When $L \ll L_s$, the backing layer can be regarded as being rigid, and the energy release rate comes from the elasticity of the soft layer, $G = h\tau^2/2\mu$. When $L \gg L_s$, much of the soft layer shears negligibly, and the energy release rate comes from the elasticity of the backing layers, $G = H\sigma^2/4E$. Between these two limits, we propose to add the two limiting results:

$$G = \frac{H}{4E}\left(\frac{F}{wH}\right)^2 + \frac{h}{2\mu}\left(\frac{F}{wL}\right)^2. \tag{10}$$

This result is used to calculate the steady-state energy release rate for samples of any length, so long as the length of the crack and the sample length are large compared to the thickness of the soft layer.

We do uniaxial tension test to determine Young's modulus of the backing layer, giving $E = 4.2 \pm 0.2$ GPa. Inserting $E = 4.2$ GPa, $H = 50$ μm, $h = 9$ mm, and $\tilde{\mu} = 2.634$ kPa into Eq. (3), we can obtain the shear lag length $L_s = 84.7$ cm.

4.2. Finite element analysis of the effect of the backing layer elasticity

Further, we use finite element software ABAQUS to ascertain that Eq. (10) does approximately represent the energy release rate for samples of intermediate lengths. We calculate the energy release rate as a function of the sample length at various crack lengths. The energy release rate G normalized by the contribution of backing layer elasticity, $\frac{H}{4E}(\frac{F}{wH})^2$, is plotted as a function of normalized sample length, L/L_s, at various normalized crack lengths, c/h (Fig. 9). The finite element calculation is consistent with the shear lag model when the crack length is large compared to the thickness. It confirms that the elasticity of the backing layer dominates the steady-state energy release rate when L is large compared to L_s.

4.3. Experimental measurement of adhesion toughness

We experimentally measure the adhesion toughness by introducing a crack to the interface between PAA and PAAm with a crack length c, as a function of the length L (Fig. 10).

We fix the thickness $h = 9$ mm and the width $w = 2$ cm. To guarantee a steady-state fracture, the crack length c is made to be $3h$. The results show that the adhesion toughness is independent of the length. Using Eq. (10), we can calculate the steady-state energy release rate. The average energy release rate at steady state is 37 J/m^2, which is similar to that of the short samples (Fig. 7). It confirms that adhesion toughness is constant and independent of the thickness and length.

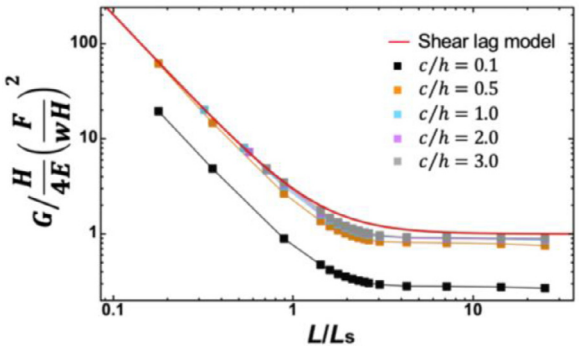

Fig. 9. Normalized energy release rate $G/\frac{H}{4E}(\frac{F}{wH})^2$ as a function of normalized sample length L/L_s at various normalized crack lengths c/h. The finite element calculation and the shear lag model are consistent when the crack length is large compared to the thickness.

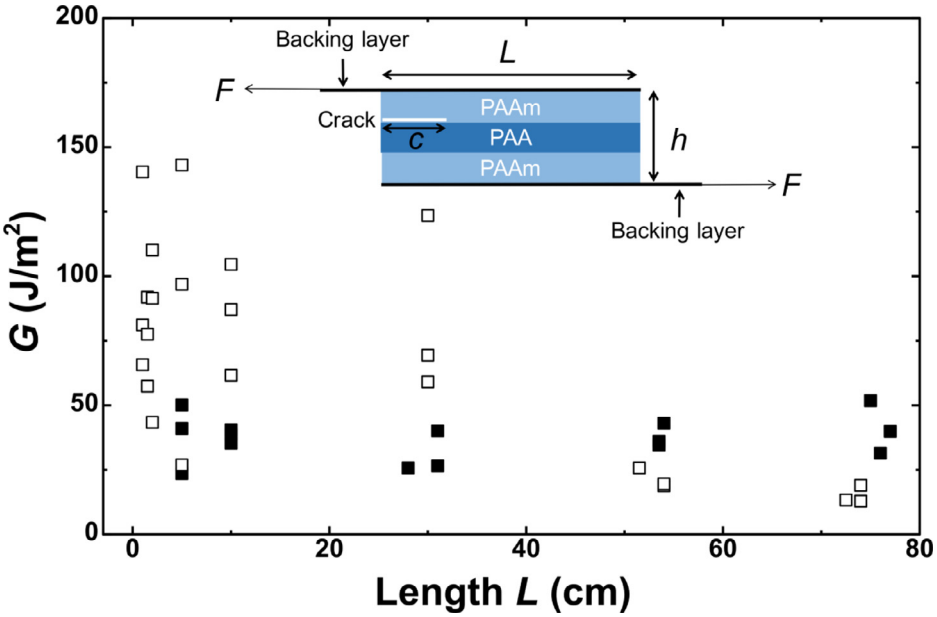

Fig. 10. Adhesion toughness measured using samples of various lengths. The thickness and the width are 9 mm and 2 cm, respectively. To ensure steady state, the crack length is made to be large compared to the thickness. In this case, $c = 3h = 2.7$ cm. The empty squares represent the measured adhesion toughness of samples with no pre-cut crack.

Similar to the cases of short samples, we use Eq. (10) to calculate the energy release rate of the cases in Fig. 1e, where no pre-cut crack is introduced. The results (empty squares in Fig. 10) show large scatters. Again, this is due to the absence of pre-cut crack. Therefore, a pre-cut crack long compared to the thickness is necessary to measure constant adhesion toughness.

In a recent paper (Golovin et al., 2019), the importance of sample length was observed in deicing. The force required to shear-off ice is proportional to the iced area when the iced area is small, but is independent of the iced area when the iced area is large. These authors did not report the effect of the pre-cut crack. Here we observe significant effect of pre-cut crack, possibly because the soft layer used in our experiments is thick, $h = 9$ mm. We also note another difference between the paper on deicing and the work here. In the deicing paper, the transition from strength-limited deicing and toughness-limited deicing occurs at a length that relates to the interfacial strength and toughness. The transition length identified in this paper is the shear lag length, which relates to the elasticity of the soft material and the backing layer, but is independent of strength and toughness. The two works involve two different sets of materials; an in-depth comparison is beyond the scope of this paper.

5. Lap shear with rigid substrates

The experiments above use thin plastic films as backing layers. This experimental procedure is often used in the literature (Ni et al., 2019; Roy et al., 2015; Vakalopoulos et al., 2015; Yuk et al., 2019). We now compare this experimental approach

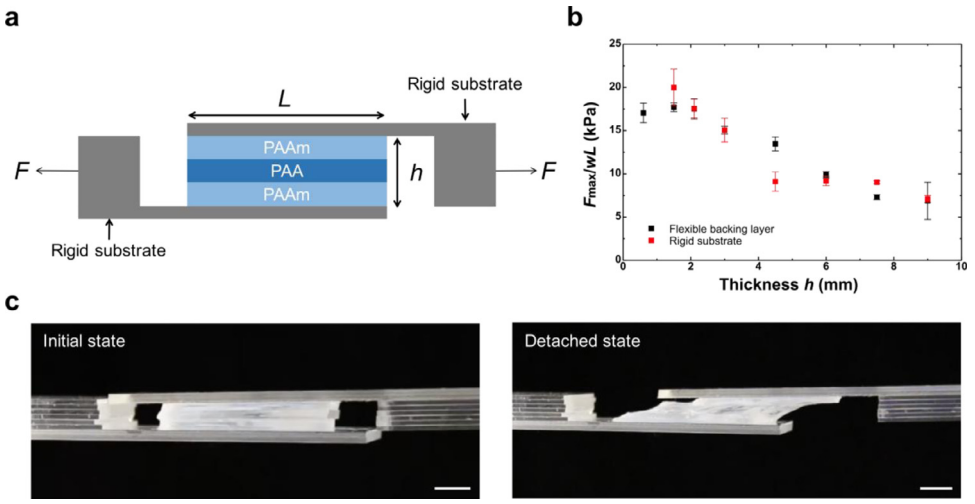

Fig. 11. Lap shear using rigid substrates. (a) Experimental setup. A PAA hydrogel (pH=1.5) is sandwiched by two PAAm hydrogels (pH=3.5), glued to rigid acrylic substrate. The three-layered sample has the dimension: the length L, the width w, and the thickness h. (b) Comparison between our approach (backing layer) and the standard setup (rigid substrate). The results are similar. (c) Photo image of a sample in initial state and detached state. The rigid substrates do not rotate. Scale bar is 1 cm.

with a standard lap-shear test (ASTM F2255-05). In the experimental setup that uses inextensible but flexible backing layer, rotation exists and the stress state is not only in shear (Fig. 1c). By comparison, in experiment using rigid substrate, such rotation is avoided (Fig. 11a).

To make comparisons, we make all the parameters identical, including the geometry of the samples and the loading rate. We employ the standard lap-shear test to measure the adhesion strength between PAA and PAAm (red dots) as a function of the thickness, and compare with the results obtained by our experimental setup (black dots) (Fig. 11b). The results are similar, confirming the validity of our results and findings. As a loading machine pulls the two rigid substrates, the sample does not rotate (Fig. 11c, Video 2).

In the lap shear experiments, we often observe interfacial failure, rather than cohesive failure (Video 1 and Video 2). After experiments, the sample surface is relatively smooth. We did not observe cavitation, pillars, and stick slip.

6. Experimental section

6.1. Preparation of hydrogels

All chemicals were purchased, including acrylic acid (AA; Sigma-Aldrich, 147230), acrylamide (AAm; Sigma-Aldrich, A8887), N,N'-methylenebisacrylamide (MBAA; Sigma-Aldrich, M7279), and alpha-ketoglutaric acid (Sigma-Aldrich, 75890).

For polyacrylic acid (PAA) hydrogel, we prepared the precursor by mixing an aqueous solution of AA monomer (1.736 mol/L) with MBAA (0.14% the weight of AA) as the crosslinker, and alpha-ketoglutaric acid (0.2% the weight of AA) as the photoinitiator. Then, we poured the precursor into a plastic mold glued on the acrylic substrate. A glass sheet was used to seal the mold, where the solutions gelled under UV. The pH of PAA hydrogel precursor was 1.5, measured by pH test strips,

For polyacrylamide (PAAm) hydrogel, we prepared the precursor by mixing an aqueous solution of AAm monomer (1.916 mol/L) with MBAA (0.058% the weight of AAm) as the crosslinker, and alpha-ketoglutaric acid (0.2% the weight of AAm) as the photoinitiator. Then, we poured the precursor into a plastic mold glued on the acrylic substrate. A glass sheet was used to seal the mold, where the solutions gelled under UV. The pH of PAAm hydrogel precursor was 3.5, measured by pH test strips.

6.2. Lap-shear test

To characterize hydrogel adhesion using lap-shear test, we prepared PAA hydrogels and PAAm hydrogels with the same sample size. We used cyanoacrylate (krazy glue) to glue PAAm hydrogels to inextensible polyester films as the backing layers (50 μm thickness; McMaster Carr). Since the PAAm hydrogels were acidic, their surfaces were neutralized by applying a few drops of 0.1 mol/L $NaHCO_3$ (Sigma-Aldrich, S5761) solution and then dried by blowing air before using cyanoacrylate. We then made a PAA hydrogel sandwiched by two PAAm hydrogels. Immediately after that, a weight of 500 g was applied to the sample for 10 min before the test. Then, the three-layered sample with backing layers was loaded by a tensile machine (Instron 5966; 100 N load cell) using lap-shear test. The loading rate was 10 cm/min. The shear strength was calculated by the maximum force in the force-displacement curve divided by the initial area of the sample.

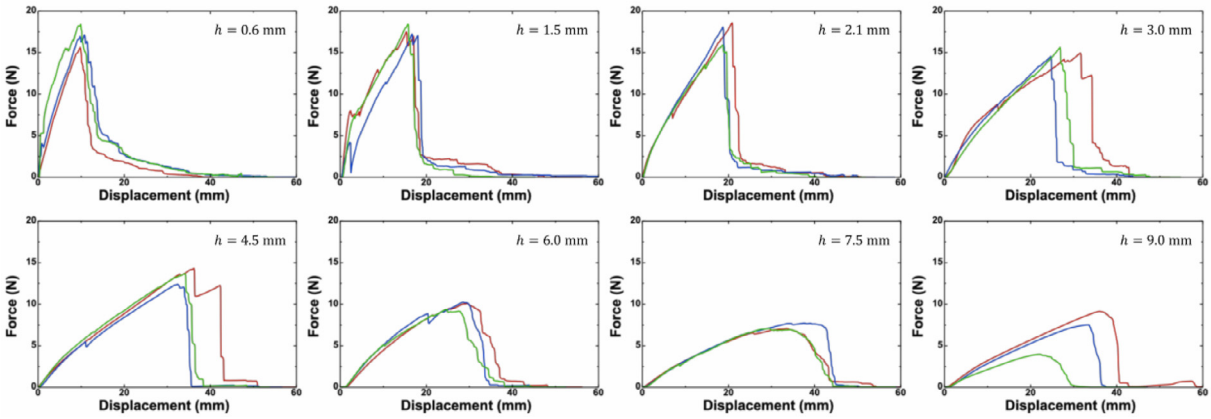

Fig. 12. Force-displacement curves of the lap-shear test of various thicknesses. The length L and the width w are fixed as 5 cm and 2 cm, respectively.

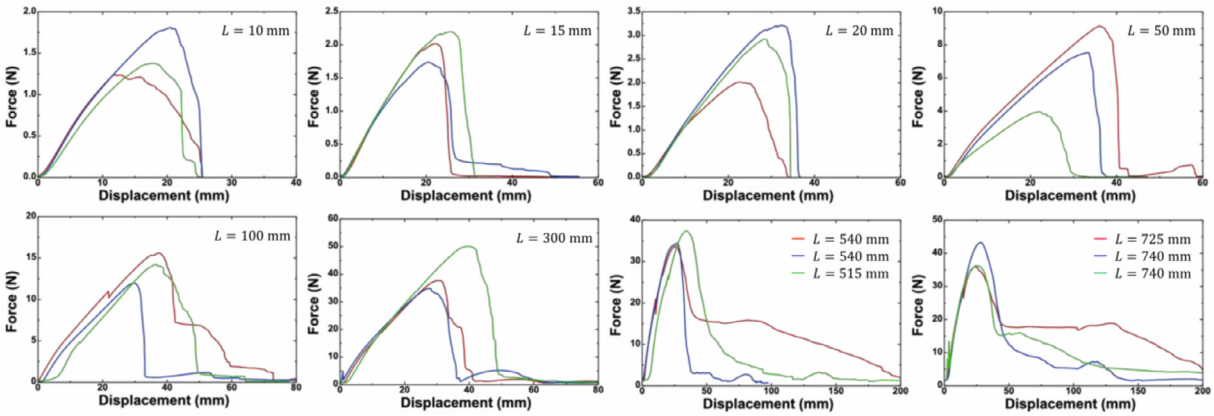

Fig. 13. Force-displacement curves of the lap-shear test of various lengths. The width w and thickness h are fixed as 2 cm and 9 mm, respectively.

6.3. Force-displacement curve

We characterize the adhesion between PAA and PAAm by lap-shear test (Fig. 1a) and measure the force-displacement curves of thickness 0.6 mm, 1.5 mm, 2.1 mm, 3.0 mm, 4.5 mm, 6.0 mm, 7.5 mm, and 9.0 mm, using three samples for each thickness (Fig. 12).

We also measure the force-displacement curves of length 10 mm, 15 mm, 20 mm, 50 mm, 100 mm, 300 mm, ~ 532 mm, and ~ 735 mm, using three samples for each length (Fig. 13).

7. Conclusion

We have studied the mechanics of lap shear and shown that the adhesion strength so determined is constant only when the sample is thin and short enough. When the sample is thick compared to the fractoadhesive length, the effect of stress concentration at the corner prevails, and the adhesion strength decreases as the sample thickness increases. When the sample is long compared to the shear lag length, the backing layers deform appreciably, much of the soft layer is nearly undeformed, and the adhesion strength decreases as the sample length increases. We develop an analytical expression for the energy release rate for samples with pre-cut crack large compared to the thickness. This expression enables us to use lap shear to measure adhesion toughness. Our data confirm that adhesion toughness is independent of sample length. This work studies the applicability of adhesion strength and adhesion toughness. The large variation in shear strength with respect of sample thickness and length serves as a caution in comparing data reported in the literature.

Declaration of competing interest

The authors declare no competing interest.

Acknowledgement

The work at Harvard is supported by NSF MRSEC (DMR-14–20570), United States. X. Yang is supported by China Scholarship Council as a visiting student at Harvard University.

Supplementary materials

Supplementary material associated with this article can be found, in the online version, at doi:10.1016/j.jmps.2020.103988.

Appendix A

Additional results of finite element calculation

In the calculation, we conduct parametric studies and find that: (i) when the sample length is short compared to the shear lag length, correction of crack length is needed in shear stress calculation to reach steady state; (ii) when the sample length is large compared to the shear lag length, the effect of the backing layer elasticity is significant.

In the calculation, the sample thickness h and the length of the backing layer are set to be 4.5 mm and 750 mm, respectively, and the introduced pre-cut crack length c varies from 0.01 h to 3 h. To simplify the calculation, we replace the three-layered composite by a homogeneous hydrogel with a shear modulus $\bar{\mu} = 2.634$ kPa.

A.1 Correction of crack length in shear stress calculation

First of all, we make the sample length $L = 100$ mm and the Young's modulus of the backing layer $E = 920$ MPa, and calculate the normalized energy release rate $G/h\tau^2/2\bar{\mu}$ as a function of normalized crack length c/h at various normalized shear stresses $\tau/\bar{\mu}$ (Fig. A1). It shows that the normalized energy release rate increases as the normalized crack length increases. However, no steady state is reached (Fig. A1a). This is because the length L is not large enough to ensure homogeneous stress distribution. To reach steady state, the correction of crack length is necessary to calculate the shear stress τ (Fig. A1b). In other words, the shear stress is calculated by $F/w(L-c)$, rather than F/wL, where F is the applied load and w is the width of the sample.

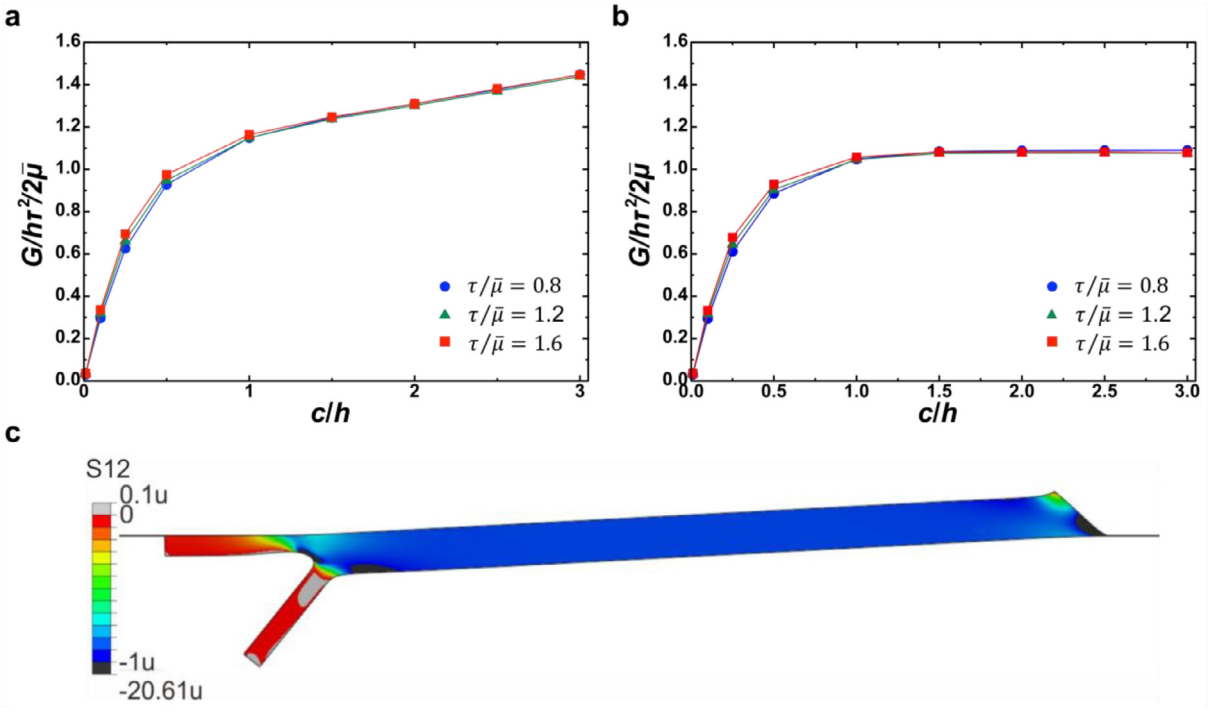

Fig. A1. Normalized energy release rate $G/h\tau^2/2\bar{\mu}$ as a function of normalized crack length c/h at various normalized shear stresses $\tau/\bar{\mu}$. (a) Results without correction of crack length, where the average shear stress τ is calculated by F/wL. No steady state is achieved. (b) Results with correction of crack length, where the shear stress is calculated by $F/w(L-c)$. (c) Shear stress (S12) distribution in the soft layer when $c/h = 3$ and $\tau/\bar{\mu} = 1$. $L = 100$ mm and $E = 920$ MPa.

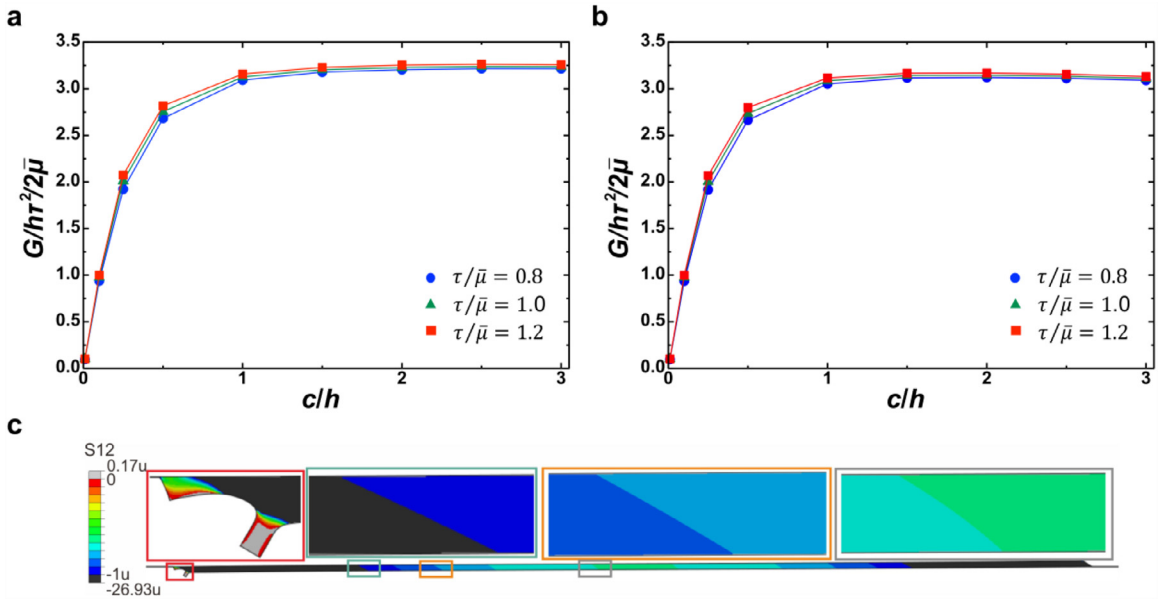

Fig. A2. Normalized energy release rate $G/h\tau^2/2\bar{\mu}$ as a function of normalized crack length c/h at various normalized shear stresses $\tau/\bar{\mu}$. Steady state is reached in both cases: (a) without correction of crack length; (b) with correction of crack length. (c) Shear stress (S12) distribution in the soft layer when $c/h = 1$ and $\tau/\bar{\mu} = 1$. $L = 700$ mm and $E = 920$ MPa.

To confirm it, we plot the shear stress distribution in the soft layer with a pre-cut crack long compared to the sample thickness, $c/h = 3$ (Fig. A1c). It shows that the parts above and under the crack surface have approximately negligible shear stress, compared with the shear stress in the soft layer. As a result, when the crack length is comparable to the sample length, we need to correct the crack length in shear stress calculation to reach steady state.

Further, we do the same calculation with the same parameters, but make the length L large compared to the shear lag length, $L = 700$ mm (Fig. A2). In this case, the crack length c is much smaller than the length L, such that the steady state is reached when $c/h \geq 1$ (Fig. A2a and A2b).

In this case, the normalized steady state energy release rate increases to 3, because the backing layers cannot be assumed to be rigid. To ascertain that, we plot the shear stress distribution in the soft layer with $c/h = 1$ (Fig. A2c), indicating an inhomogeneous shear stress distribution. It is due to the fact that the backing layer is not rigid, but deforms appreciably. To further confirm it, we compare the energy release rate calculated by finite element with that calculated by Eq. (10) (Table A1). The finite element calculation is consistent with the theoretical prediction when $L = 100$ mm, but has some difference when $L = 700$ mm. Therefore, the effect of the backing layer elasticity needs to be carefully considered.

A.2 Effect of the backing layer elasticity

To make the backing layer rigid, we make the Young's modulus of the backing layer 100 times larger, $E = 92$ GPa, keep the length $L = 700$ mm, and do the same calculation (Fig. A3).

In this case, the correction of crack length becomes less important in shear stress calculation and the normalized energy release rate reaches 1 at steady state (Fig. A3a and A3b). Also, the shear stress is uniformly distributed in the soft layer (Fig. A3c).

We further confirm the effect of the backing layer elasticity by comparing the energy release rate calculated by finite element and that calculated by Eq. (10) (Table A2). When the sample length is large compared to the shear lag length and the backing layer is rigid, the finite element calculation and the theoretical prediction are consistent.

Table A1
Energy release rate at steady state ($E = 920$ MPa).

	FEM	Eq. (10)
Energy release rate (J/m^2) when $L = 100$ mm	9.19	8.98
Energy release rate (J/m^2) when $L = 700$ mm	27.04	34.46

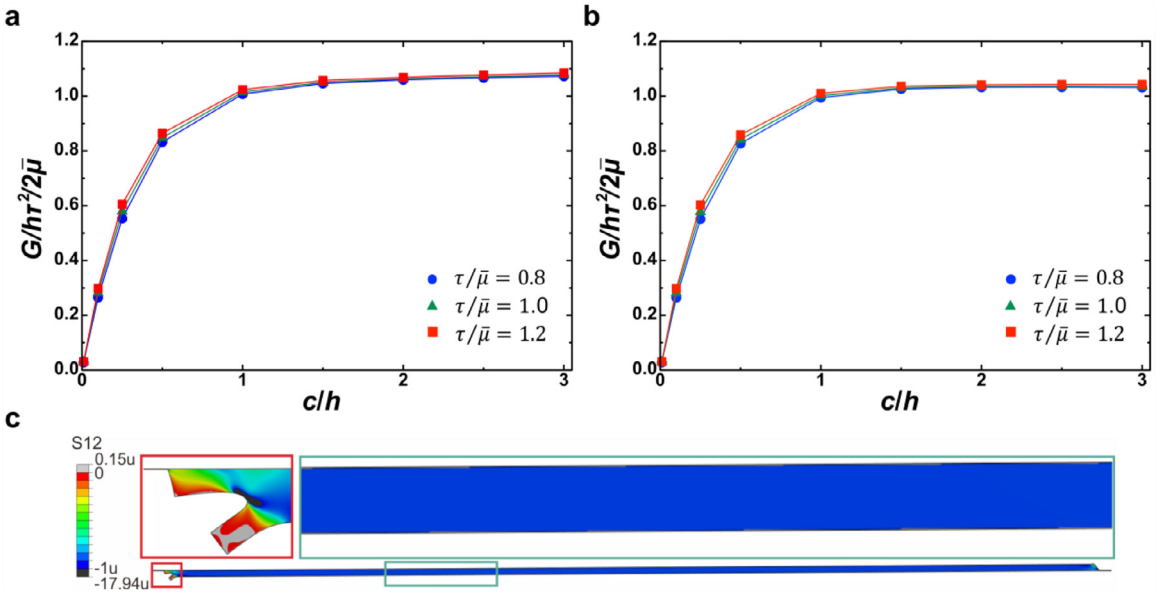

Fig. A3. Normalized energy release rate $G/h\tau^2/2\bar{\mu}$ as a function of normalized crack length c/h at various normalized shear stresses $\tau/\bar{\mu}$. Steady state is reached in both cases: (a) without correction of crack length; (b) with correction of crack length. The calculated energy release rate is consistent with that obtained from the theoretical prediction. (c) Shear stress (S12) distribution in the soft layer when $c/h = 1$ and $\tau/\bar{\mu} = 1$. The stress distribution is homogeneous. $L = 700$ mm and $E = 92$ GPa.

Table A2
Energy release rate at steady state ($L = 700$ mm).

	FEM	Eq. (10)
Energy release rate (J/m^2) when E = 920 MPa	27.04	34.46
Energy release rate (J/m^2) when E = 92 GPa	9.12	8.80

References

Bhagat, V., Becker, M.L., 2017. Degradable adhesives for surgery and tissue engineering. Biomacromolecules 18, 3009–3039.
Blacklow, S.O., Li, J., Freedman, B.R., Zeidi, M., Chen, C., Mooney, D.J., 2019. Bioinspired mechanically active adhesive dressings to accelerate wound closure. Sci. Adv. 5, eaaw3963.
Chen, B., Yang, J., Bai, R., Suo, Z., 2019. Molecular staples for tough and stretchable adhesion in integrated soft materials. Adv. Healthc. Mater. 8, 1900810.
Chen, C., Wang, Z., Suo, Z., 2017. Flaw sensitivity of highly stretchable materials. Extreme. Mech. Lett. 10, 50–57.
Cheng, S., Narang, Y.S., Yang, C., Suo, Z., Howe, R.D., 2019. Stick-on large-strain sensors for soft robots. Adv. Mater. Interfaces. 6, 1900985.
Cox, H.L., 1952. The elasticity and strength of paper and other fibrous materials. Br. J. Appl. Phys. 3, 72–79.
da Silva, L.F.M., das Neves, P.J.C., Adams, R.D., Spelt, J.K., 2009a. Analytical models of adhesively bonded joints—Part I: literature survey. Int. J. Adhes. Adhes. 29, 319–330.
da Silva, L.F.M., das Neves, P.J.C., Adams, R.D., Wang, A., Spelt, J.K., 2009b. Analytical models of adhesively bonded joints—Part II: comparative study. Int. J. Adhes. Adhes. 29, 331–341.
da Silva, L.F.M., Rodrigues, T.N.S.S., Figueiredo, M.A.V., de Moura, M.F.S.F., Chousal, J.A.G., 2006. Effect of adhesive type and thickness on the lap shear strength. J. Adhes. 82, 1091–1115.
Ebnesajjad, S., Landrock, A.H., 2014. Adhesives Technology Handbook. William Andrew.
Gao, Y., Wu, K., Suo, Z., 2018. Photodetachable adhesion. Adv. Mater 31, 1806948.
Ghareeb, A., Elbanna, A., 2019. Extreme enhancement of interfacial adhesion by bulk patterning of sacrificial cuts. Extreme. Mech. Lett. 28, 22–30.
Golovin, K., Dhyani, A., Thouless, M.D., Tuteja, A., 2019. Low–interfacial toughness materials for effective large-scale deicing. Science 364, 371–375.
Grant, L.D.R., Adams, R.D., da Silva, L.F.M., 2009. Experimental and numerical analysis of single-lap joints for the automotive industry. Int. J. Adhes. Adhes. 29, 405–413.
Hofman, A.H., van Hees, I.A., Yang, J., Kamperman, M., 2018. Bioinspired underwater adhesives by using the supramolecular toolbox. Adv. Mater. 30, 1704640.
Hong, Y., Zhou, F., Hua, Y., Zhang, X., Ni, C., Pan, D., Zhang, Y., Jiang, D., Yang, L., Lin, Q., Zou, Y., Yu, D., Arnot, D.E., Zou, X., Zhu, L., Zhang, S., Ouyang, H., 2019. A strongly adhesive hemostatic hydrogel for the repair of arterial and heart bleeds. Nat. Commun. 10, 2060.
Huang, Y., King, D.R., Sun, T.L., Nonoyama, T., Kurokawa, T., Nakajima, T., Gong, J.P., 2017. Energy-dissipative matrices enable synergistic toughening in fiber reinforced soft composites. Adv. Funct. Mater. 27, 1605350.
Hui, C.-Y., Liu, Z., Minsky, H., Creton, C., Ciccotti, M., 2018. Mechanics of an adhesive tape in a zero degree peel test: effect of large deformation and material nonlinearity. Soft Matter 14, 9681–9692.
Jeevi, G., Nayak, S.K., Abdul Kader, M., 2019. Review on adhesive joints and their application in hybrid composite structures. J. Adhes. Sci. Technol. 33, 1497–1520.
Kafkalidis, M.S., Thouless, M.D., 2002. The effects of geometry and material properties on the fracture of single lap-shear joints. Int. J. Solids. Struct. 39, 4367–4383.
Kendall, K., 1975. Cracking of short lap joints. J. Adhes. 7, 137–140.
Li, C., Yang, H., Suo, Z., Tang, J., 2020. Fatigue-resistant elastomers. J. Mech. Phys. Solids 134, 103751.

Li, J., Celiz, A.D., Yang, J., Yang, Q., Wamala, I., Whyte, W., Seo, B.R., Vasilyev, N.V., Vlassak, J.J., Suo, Z., Mooney, D.J., 2017. Tough adhesives for diverse wet surfaces. Science 357, 378–381.
Li, W., Liu, X., Deng, Z., Chen, Y., Yu, Q., Tang, W., Sun, T.L., Zhang, Y.S., Yue, K., 2019. Tough bonding, on-demand debonding, and facile rebonding between hydrogels and diverse metal surfaces. Adv. Mater. 31, 1904732.
Liu, J., Yang, C., Yin, T., Wang, Z., Qu, S., Suo, Z., 2019a. Polyacrylamide hydrogels. II. elastic dissipater. J. Mech. Phys. Solids 133, 103737.
Liu, Q., Nian, G., Yang, C., Qu, S., Suo, Z., 2018. Bonding dissimilar polymer networks in various manufacturing processes. Nat. Commun. 9, 846.
Liu, Z., Minsky, H., Creton, C., Ciccotti, M., Hui, C.-Y., 2019b. Mechanics of zero degree peel test on a tape—effects of large deformation, material nonlinearity, and finite bond length. Extreme. Mech. Lett. 32, 100518.
Mehdizadeh, M., Yang, J., 2013. Design strategies and applications of tissue bioadhesives. Macromol. Biosci. 13, 271–288.
Mojdehi, A.R., Holmes, D.P., Dillard, D.A., 2017. Friction of extensible strips: an extended shear lag model with experimental evaluation. Int. J. Solids. Struct. 124, 125–134.
Ni, X., Chen, C., Li, J., 2019. Interfacial fatigue fracture of tissue adhesive hydrogels. Extreme. Mech. Lett. 34, 100601.
Ritchie, R.O., 2011. The conflicts between strength and toughness. Nat. Mater. 10, 817–822.
Rose, S., Prevoteau, A., Elzière, P., Hourdet, D., Marcellan, A., Leibler, L., 2014. Nanoparticle solutions as adhesives for gels and biological tissues. Nature 505, 382–385.
Roy, C.K., Guo, H.L., Sun, T.L., Ihsan, A.B., Kurokawa, T., Takahata, M., Nonoyama, T., Nakajima, T., Gong, J.P., 2015. Self-adjustable adhesion of polyampholyte hydrogels. Adv. Mater. 27, 7344–7348.
Skeist, I., 1990. Handbook of Adhesives (1990). Van Nostrand Reinhold, New York, NY.
Steck, J., Yang, J., Suo, Z., 2019. Covalent topological adhesion. ACS Macro. Lett. 8, 754–758.
Taib, A.A., Boukhili, R., Achiou, S., Gordon, S., Boukehili, H., 2006. Bonded joints with composite adherends. Part I. Effect of specimen configuration, adhesive thickness, spew fillet and adherend stiffness on fracture. Int. J. Adhes. Adhes. 26, 226–236.
Vakalopoulos, K.A., Wu, Z., Kroese, L., Kleinrensink, G.-J., Jeekel, J., Vendamme, R., Dodou, D., Lange, J.F., 2015. Mechanical strength and rheological properties of tissue adhesives with regard to colorectal anastomosis: an ex vivo study. Ann. Surg. 261, 323–331.
Wang, Y., Jia, K., Xiang, C., Yang, J., Yao, X., Suo, Z., 2019a. Instant, tough, noncovalent adhesion. ACS Appl. Mater. Interfaces 11, 40749–40757.
Wang, Z., Xiang, C., Yao, X., Le Floch, P., Mendez, J., Suo, Z., 2019b. Stretchable materials of high toughness and low hysteresis. Proc. Natl. Acad. Sci. USA. 116, 5967–5972.
Wirthl, D., Pichler, R., Drack, M., Kettlguber, G., Moser, R., Gerstmayr, R., Hartmann, F., Bradt, E., Kaltseis, R., Siket, C.M., Schausberger, S.E., Hild, S., Bauer, S., Kaltenbrunner, M., 2017. Instant tough bonding of hydrogels for soft machines and electronics. Sci. Adv. 3, e1700053.
Xia, S., Ponson, L., Ravichandran, G., Bhattacharya, K., 2012. Toughening and asymmetry in peeling of heterogeneous adhesives. Phys. Rev. Lett. 108, 196101.
Xiang, C., Wang, Z., Yang, C., Yao, X., Wang, Y., Suo, Z., 2020. Stretchable and fatigue-resistant materials. Materials Today 34, 7–16.
Yang, C., Yin, T., Suo, Z., 2019a. Polyacrylamide hydrogels. I. Network imperfection. J. Mech. Phys. Solids. 131, 43–55.
Yang, H., Li, C., Tang, J., Suo, Z., 2019b. Strong and degradable adhesion of hydrogels. ACS Appl. Bio. Mater. 2, 1781–1786.
Yang, J., Bai, R., Chen, B., Suo, Z., 2019c. Hydrogel adhesion: a supramolecular synergy of chemistry, topology, and mechanics. Adv. Funct. Mater. 30, 1901693.
Yang, J., Bai, R., Suo, Z., 2018. Topological adhesion of wet materials. Adv. Mater. 30, 1800671.
Yang, X., Yang, C., Liu, J., Yao, X., Suo, Z., 2020. Topological prime. Sci. China. Technol. Sci.
Yao, X., Liu, J., Yang, C., Yang, X., Wei, J., Xia, Y., Gong, X., Suo, Z., 2019. Hydrogel paint. Adv. Mater. 31, 1903062.
Yu, Y., Yuk, H., Parada, G.A., Wu, Y., Liu, X., Nabzdyk, C.S., Youcef-Toumi, K., Zang, J., Zhao, X., 2019. Multifunctional “hydrogel skins” on diverse polymers with arbitrary shapes. Adv. Mater. 31, 1807101.
Yuk, H., Lin, S., Ma, C., Takaffoli, M., Fang, N.X., Zhao, X., 2017. Hydraulic hydrogel actuators and robots optically and sonically camouflaged in water. Nat. Commun. 8, 14230.
Yuk, H., Varela, C.E., Nabzdyk, C.S., Mao, X., Padera, R.F., Roche, E.T., Zhao, X., 2019. Dry double-sided tape for adhesion of wet tissues and devices. Nature 575, 169–174.
Yuk, H., Zhang, T., Lin, S., Parada, G.A., Zhao, X., 2015. Tough bonding of hydrogels to diverse non-porous surfaces. Nat. Mater. 15, 190.
Yuk, H., Zhang, T., Parada, G.A., Liu, X., Zhao, X., 2016. Skin-inspired hydrogel–elastomer hybrids with robust interfaces and functional microstructures. Nat. Commun. 7, 12028.
Zhu, W., Chuah, Y.J., Wang, D.-A., 2018. Bioadhesives for internal medical applications: a review. Acta. Biomater. 74, 1–16.